Pathfinder PIC Ion Chip, v1.3

Initial Design Sketch

Jonathan Feasby
Pathfinder Quantum Technologies

May 31, 2026

Abstract

We here present a preliminary design of a photonic-integrated ion trap chip for a hybrid-locality architecture, suitable for scalable quantum information processing. The chip integrates two planar ion-trap arrays fabricated above a photonic integrated circuit (PIC). Each array contains a 3-ion Coulomb crystal, with one ion acting as a communication ion and the remaining ions acting as memory ions. The intended architecture combines two different forms of entanglement: (i) **local entanglement** inside each array using motional entanglement gates in the Mølmer–Sørensen (MS) gate family, and (ii) **non-local entanglement** between arrays, using photon-mediated time-bin entanglement. We use both protocols to sidestep the ion-relocation constraints of shuttling architectures. The ion species assumed in this design is $^{138}Ba^{+}$, chosen due to its successful demonstration in previous trapped-ion experiments, and because the relevant transition wavelengths avoid fabrication difficulties associated with waveguides in the deep-ultraviolet regime.

1. Protocol and Purpose

Our design expands the time-bin photon-mediated entanglement protocol demonstrated in experiments from Duke, Oxford, and others (Saha et al. 2025; Stephenson et al. 2020; Knollmann et al. 2024) into a platform for generalised quantum computation.

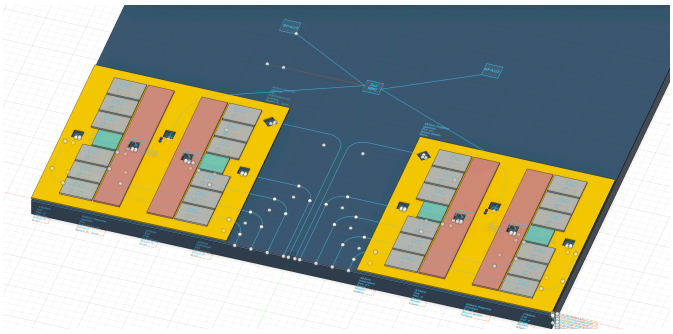

Figure 1: CAD sketch of the chip.

We propose a hybrid-locality architecture:

- Inside a single ion chain, entanglement is effected through motional coupling.
- Between separate ion chains, entanglement is effected via the correlation of photonic emission time with the state of the emitting ion ("time-bin" entanglement) (Saha et al. 2025).

Photon-mediated entanglement requires repeated optical excitation, which is destructive to a qubit state being preserved for computation. An ion storing a computational state $|\psi\rangle$ should therefore be distinct from the ion repeatedly excited for photon generation.

Instead, each array splits its ions into two roles: a communication ion that interfaces with the photonic network, and memory ions that store computational states. When a non-local operation is needed, the communication ion is used to create a remote entangled link, which is then consumed to teleport the relevant quantum state to the target array (Bennett et al. 1993; Riebe et al. 2004).

There is nothing physically distinguishing the communication ion from the memory ions; the distinction is purely functional, set by the role each is assigned and the state it carries.

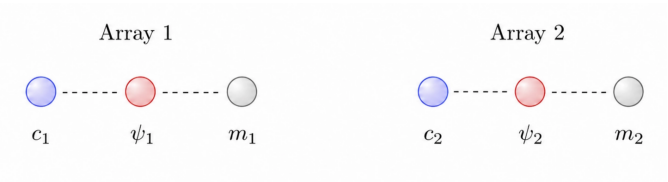

Figure 2: Two arrays, each containing a communication ion c, a target qubit state $|\psi\rangle$, and a memory ion m.

A Bell state is then generated between the communication ions.

Figure 3: Bell pair $|\Psi^{\pm}\rangle$ generated between the communication ions c_1 and c_2.

A Bell state measurement (BSM) is then performed on $|\psi_2\rangle$ and c_2, the results of which inform the gates performed on c_1.

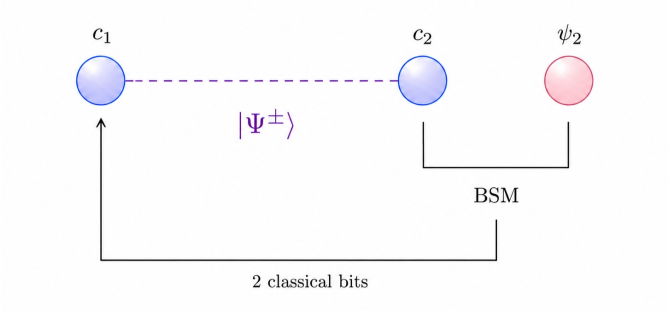

Figure 4: Bell-state measurement on $|\psi_2\rangle$ and c_2; two classical bits are fed forward to c_1.

After the operations corresponding to the two classical bits are applied to qubit c_1, its state is transformed to the target state $|\psi_2\rangle$, meaning that the two target states $[|\psi_1\rangle, |\psi_2\rangle]$ are in the same array, and can be entangled with high-fidelity gates. The current qubit array is $[|\psi_2\rangle, |\psi_1\rangle, m_1]$.

We want to keep the communication ion open for future operations, so we move $|\psi_2\rangle$ into the open memory slot m_1.

This is achieved via a local two-qubit SWAP operation (Nielsen and Chuang 2010), resulting in the final state of the qubit array:

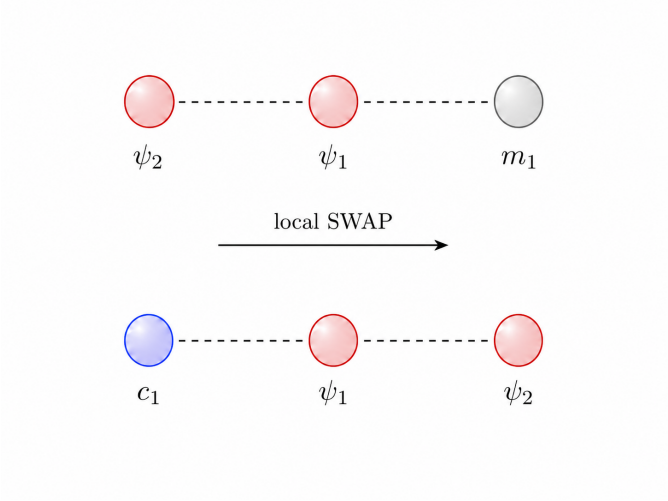

Figure 5: Local SWAP moves $|\psi_2\rangle$ into the memory slot, freeing c_1 for the next networking operation.

2. Relevant Atomic Transitions

The $^{138}Ba^{+}$ species supports an optical qubit on the following transitions:

- 493nm: $6^2S_{1/2} \leftrightarrow 6^2P_{1/2}$
- 650nm: $5^2D_{3/2} \leftrightarrow 6^2P_{1/2}$
- 614nm: $5^2D_{5/2} \leftrightarrow 6^2P_{3/2}$
- 1762nm: $6^2S_{1/2} \leftrightarrow 5^2D_{5/2}$

We define the qubit states as:

$$|\downarrow\rangle = 6^2S_{1/2}, \qquad |\uparrow\rangle = 5^2D_{5/2}.$$

The 1762nm laser therefore drives the coherent optical qubit transition, the 493nm beam is used for excitation, fluorescence, readout, and cooling-related operations, and the 650nm and 614nm beams act as repump/deshelving beams.

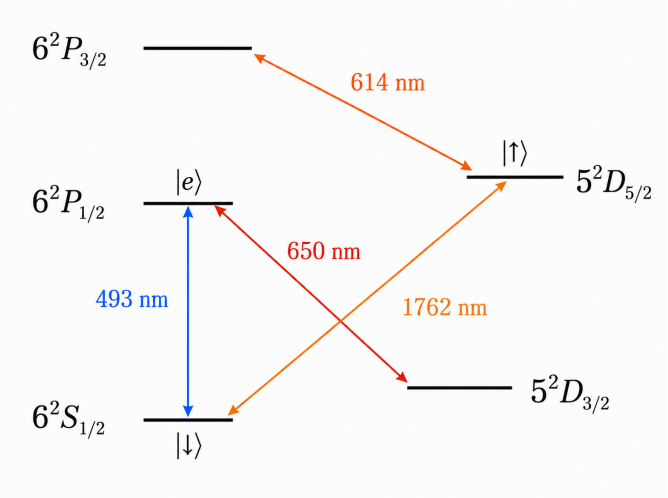

Figure 6: Level diagram of $^{138}Ba^{+}$ with the relevant transitions and qubit-state assignment.

3. Material Stack

The chip is built on a silicon base with an integrated photonic layer below the surface-electrode ion trap. The layers and their thicknesses are shown below.

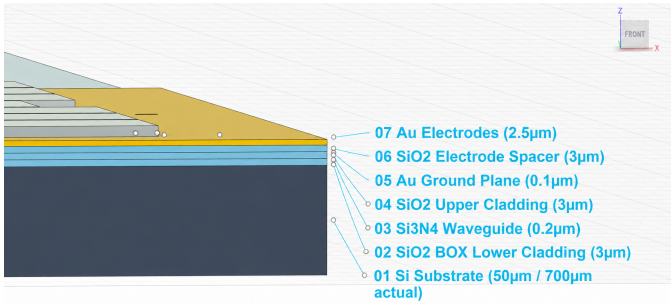

Figure 7: Cross-section of the material stack with layer labels and thicknesses.

The chip is best understood as a surface-electrode ion trap built above an embedded Si_3N_4 photonic circuit. Importantly, the photonic layer is not a continuous slab of Si_3N_4; rather, it consists of patterned Si_3N_4 waveguides,

splitters, and gratings embedded inside SiO_2 cladding. In the CAD model this is shown as a single Si_3N_4 waveguide layer for readability, but physically the waveguides are high-index cores inside a lower-index oxide cladding. The silicon substrate is trimmed to 50 µm in the CAD design for visibility (the real depth is 700 µm).

4. Waveguides

Waveguides fall into two categories:

- **Delivery** waveguides carry light onto the ions, and divide further into *individual* addressing (a single targeted ion) and *global* addressing (all ions at once).
- **Collection** waveguides carry emitted photons away from the ions toward detection.

Individual addressing lasers such as the 493nm beam and the 1762nm qubit laser must support the TE_{10} and TE_{20} modes, for reasons described in the next section. Global addressing lasers need only support the TE_{10} mode.

Addressing waveguides will see high photonic flux, while collection waveguides must support single-photon collection.

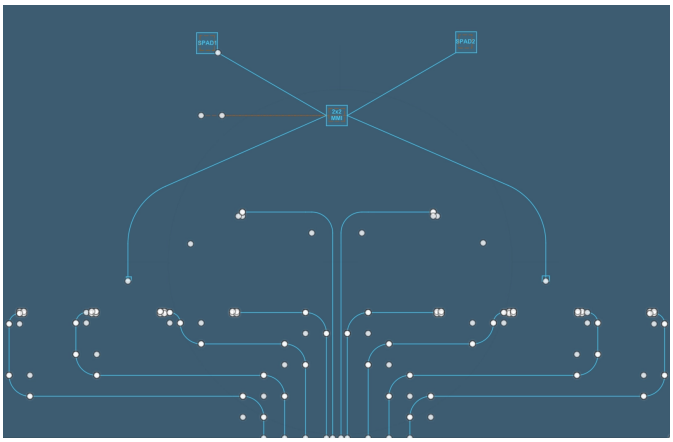

Figure 8: Top-down view of the waveguide layer. Addressing waveguides enter from the side (oriented at the bottom in this view), and collection waveguides are fed through to the entanglement region.

Addressing light enters through the bottom of the chip from a light generation module, not included in the current sketch. Photons from collection gratings are routed through a 2×2 multimode interferometer (MMI) to eliminate which-path information, as visualised in Fig. 9. Note that the light propagation through the MMI is that of a single photon; the highlighted region represents the probability density of the photon's position.

The outputs of the MMI are then sent to single-photon avalanche detectors (SPADs).

5. Grating System: Individual Addressing

In conventional free-space trapped-ion setups, individual addressing is often performed with external optics such as acousto-optic modulators (AOMs) or deflectors (AODs). Such optics are not suitable for PIC integration due to concerns surrounding optic size and alignment; a different approach is therefore required to address individual ions.

Earlier versions of the design used a simple "one ion, one grating" approach, but this proved cumbersome: each ion needed its own emitter, routing, and electrode aperture, and the layout became congested at even modest ion counts.

We instead propose the use of a compact grating-addressing scheme based on a multimode waveguide and an adjoint-optimised apodised focusing grating coupler (Momenzadeh et al. 2025). This allows a single grating structure to address multiple ion positions by controlling the modal content in the waveguide.

The supported modes behave as follows:

- When emitted via the focusing grating coupler, the TE_{10} mode produces a single-lobed, approximately Gaussian spot at the central ion.
- The TE_{20} mode produces a double-lobed pattern that illuminates both outer ions simultaneously.
- Coherent superpositions of the two modes can be tuned to place a single spot on either outer ion.

Note that the 1762nm qubit laser must support the red and blue sidebands required for MS gates.

Exact powers, waists, and pulse conditions are not yet finalised in this sketch.

6. Photon Collection

In bulk-optical systems, fluorescence photons are collected using a high-NA objective lens. In a PIC architecture, the corresponding structure is an integrated collection grating. The same grating physics can be used in reverse: a grating that emits a focused beam toward an ion can also collect light emitted from that ion. This is just optical reciprocity.

Prior work has already demonstrated successful photon collection from an ion into an integrated grating (Knollmann et al. 2025).

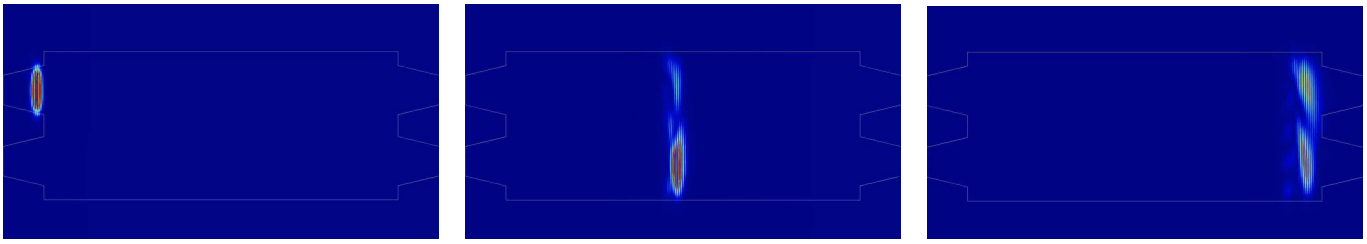

(a) Light enters the MMI through a single port.

(b) The wave propagates through the MMI region.

(c) Light exits as an equal superposition of the two exit ports.

Figure 9: Single-photon propagation through the 2×2 MMI. The highlighted region represents the probability density of the photon's position.

7. Placement of Collection Gratings

The collection gratings are placed according to two constraints.

1. **Physical layout:** The gratings must fit around the electrode geometry, the RF rails, the DC electrodes, and the optical addressing apertures.
2. **Atomic-emission constraint:** The strength of photon emission for a given light polarisation depends on the atomic transition and the direction of the quantisation axis defined by the magnetic field. Consequently, the rate of photon collection can be maximised by placing the collection grating at the optimal angle relative to the quantisation axis.

The photons targeted for collection in this setup are σ-polarised with a wavelength of 493nm. σ-polarised light from this transition is emitted most strongly parallel to the quantisation axis. This informs our placement of the collection grating (between the RF rails, above the ion chain in the photo below).

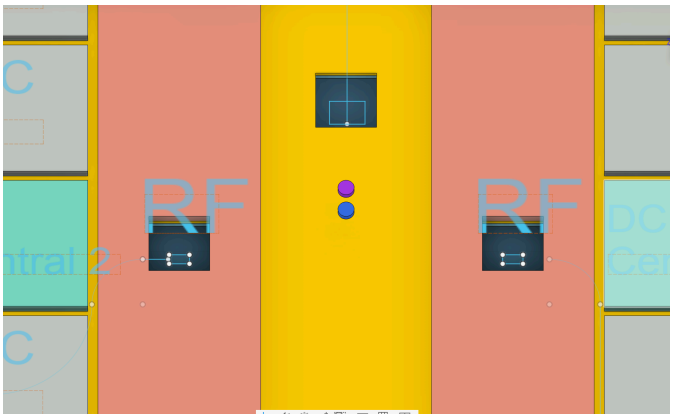

Figure 10: Collection grating layout around the trap centre, with windows through the RF/DC electrodes.

8. Electrode Apertures and ITO Covers

Any grating that emits or collects vertically needs optical access through the layers above it. The most important blockers are the metal layers: the Au ground plane and the Au electrode layer.

The current model uses square apertures above the grating couplers to preserve line-of-sight between the buried grating and the ion.

Open apertures in trap electrodes can expose dielectric and distort the local electric field, so the current design includes indium tin oxide (ITO) covers over the square grating holes, acting as transparent conductive lids.

9. To-Do List and Unimplemented Features

Below is a non-exhaustive list of chip-level parameters, features, and components not yet implemented: RF and DC wiring, EM simulations, light beam simulations, ion loading, vacuum systems, barium reservoir, photoionisation, error budgeting, parameterisation of light power requirements, optical loss modelling, and many others.

These will be implemented in future drafts.

References

Bennett, Charles H., Gilles Brassard, Claude Crépeau, Richard Jozsa, Asher Peres, and William K. Wootters. 1993. "Teleporting an Unknown Quantum State via Dual Classical and Einstein-Podolsky-Rosen Channels." *Physical Review Letters* 70: 1895–99. https://doi.org/10.1103/PhysRevLett.70.1895.

Knollmann, Felix W., Ethan Clements, Patrick T. Callahan, et al. 2024. "Integrated Photonic Structures for Photon-Mediated Entanglement of Trapped Ions." *arXiv Preprint arXiv:2401.06850*. https://arxiv.org/abs/2401.06850.

Knollmann, Felix W., Sabrina M. Corsetti, Ethan R. Clements, et al. 2025. "Collection of Fluorescence from an Ion Using Trap-Integrated Photonics." *Light: Science & Applications*, ahead of print. https://doi.org/10.1038/s41377-025-02138-9.

Momenzadeh, Melika, Ke Sun, Qiming Wu, et al. 2025. "Scalable Trapped Ion Addressing with Adjoint-Optimized Multimode Photonic Circuits." *arXiv Preprint arXiv:2505.08997*. https://arxiv.org/abs/2505.08997.

Nielsen, Michael A., and Isaac L. Chuang. 2010. *Quantum Computation and Quantum Information: 10th Anniversary Edition*. Cambridge University Press.

Riebe, M., H. Häffner, C. F. Roos, et al. 2004. "Deterministic Quantum Teleportation with Atoms." *Nature* 429: 734–37. https://doi.org/10.1038/nature02570.

Saha, Sagnik, Mikhail Shalaev, Jameson O'Reilly, et al. 2025. "High-Fidelity Remote Entanglement of Trapped Atoms Mediated by Time-Bin Photons." *Nature Communications* 16: 2533. https://doi.org/10.1038/s41467-025-57557-4.

Stephenson, L. J., D. P. Nadlinger, B. C. Nichol, et al. 2020. "High-Rate, High-Fidelity Entanglement of Qubits Across an Elementary Quantum Network." *Physical Review Letters* 124: 110501. https://doi.org/10.1103/PhysRevLett.124.110501.